

# Interpretation of EXAFS in scheelite-type $\text{AWO}_4$ ( $\text{A} = \text{Ca}, \text{Sr}, \text{Ba}$ ) compounds using molecular dynamics simulations

Aleksandr Kalinko and Alexei Kuzmin

Institute of Solid State Physics, University of Latvia, Riga, Latvia

E-mail: [akalin@latnet.lv](mailto:akalin@latnet.lv)

**Abstract.** In this work we successfully interpret the W  $\text{L}_3$ -edge EXAFS spectra in scheelite-type  $\text{AWO}_4$  ( $\text{A} = \text{Ca}, \text{Sr}, \text{Ba}$ ) compounds using a combination of classical NVT molecular dynamics (MD) and *ab initio* multiple-scattering (MS) theory. The configuration-averaged EXAFS spectra show good agreement with our room temperature experimental data supporting the reliability of the developed force-field models. The contributions from all coordination shells up to 6 Å are elucidated. The contribution of the MS effects into the total EXAFS signal in  $\text{AWO}_4$  compounds is small, being around 10%.

## 1. Introduction

Analysis and interpretation of EXAFS signals in the presence of disorder and multiple-scattering (MS) effects is a challenging task, which can be addressed by the MD-EXAFS method based on molecular dynamics (MD) simulations combined with *ab initio* EXAFS spectra calculation [1]. This method is particularly suitable to access structural information beyond the first coordination shell in crystalline materials [2, 3, 4, 5]. In this work, the MD-EXAFS method is used to clarify the contribution of the outer coordination shells and the importance of the MS effects and thermal disorder in the W  $\text{L}_3$ -edge EXAFS spectra of  $\text{AWO}_4$  ( $\text{A}=\text{Ca}, \text{Sr}, \text{Ba}$ ) tungstates.

Polycrystalline tungstates  $\text{AWO}_4$  have tetragonal (space group  $I4_1/a$ ) scheelite-type structure composed of  $[\text{WO}_4]$  tetrahedra and  $[\text{AO}_8]$  polyhedra [6, 7]. Recently they gained renewed interest for application as active media in solid state Raman lasers due to the W–O bonds have high internal vibration frequencies [8, 9]. The local atomic structure of  $\text{AWO}_4$  ( $\text{A}=\text{Ca}, \text{Sr}$ ) was studied by the W  $\text{L}_3$ -edge EXAFS spectroscopy in [10, 11, 12, 13] only within the range of the first coordination shell of tungsten. The analysis of the outer shells and the role of the multiple-scattering (MS) effects in the EXAFS spectra were not addressed. To the best of our knowledge, no EXAFS studies of  $\text{BaWO}_4$  have been performed until now.

## 2. Experimental and calculation details

Commercially available powders (99.9% purity) of  $\text{AWO}_4$  ( $\text{A}=\text{Ca}, \text{Sr}, \text{Ba}$ ) tungstates were characterized by x-ray powder diffraction and Raman spectroscopy and used in EXAFS studies.

X-ray absorption measurements were performed at the W  $\text{L}_3$  (10207 eV) edge in transmission mode at the HASYLAB DESY C1 bending-magnet beamline at 300 K. The x-ray beam intensity

**Table 1.** Force-field models for  $\text{CaWO}_4$ ,  $\text{SrWO}_4$  and  $\text{BaWO}_4$  used in the molecular dynamics simulations. Parameters for  $\text{CaWO}_4$  are from [17], whereas for  $\text{SrWO}_4$  and  $\text{BaWO}_4$  they were obtained in the present work.

CaWO <sub>4</sub>			SrWO <sub>4</sub>			BaWO <sub>4</sub>			
Buckingham potential, cutoff 14 Å									
<i>A</i> , eV	<i>ρ</i> , Å	<i>C</i> , eV Å <sup>2</sup>	<i>A</i> , eV	<i>ρ</i> , Å	<i>C</i> , eV Å <sup>2</sup>	<i>A</i> , eV	<i>ρ</i> , Å	<i>C</i> , eV Å <sup>2</sup>	
A–O	2312.0	0.2812	0.0	516.15	0.3865	0.0	534.77	0.3959	0.0
O–O	2023.0	0.2674	13.83	4634.08	0.2871	182.81	3475.78	0.2824	108.03
Morse potential, cutoff 2 Å									
<i>D<sub>e</sub></i> , eV	<i>a<sub>m</sub></i> Å <sup>−2</sup>	<i>r<sub>0</sub></i> , Å	<i>D</i> , eV	<i>a<sub>m</sub></i> Å <sup>−2</sup>	<i>r<sub>0</sub></i> , Å	<i>D</i> , eV	<i>a<sub>m</sub></i> Å <sup>−2</sup>	<i>r<sub>0</sub></i> , Å	
W–O	1.501	2.671	1.8928	0.914	3.109	1.8928	1.240	2.931	1.8928
Three-body potential, cutoff 2 Å									
<i>k</i> , eV rad <sup>−2</sup>	<i>θ<sub>0</sub></i> , deg		<i>k</i> , eV rad <sup>−2</sup>	<i>θ<sub>0</sub></i> , deg		<i>k</i> , eV rad <sup>−2</sup>	<i>θ<sub>0</sub></i> , deg		
O–W–O	2.6071	110.524		1.5266	110.524		3.0148	110.524	

was measured by two ionization chambers filled with argon and krypton gases. The higher order harmonics were effectively eliminated by detuning the double-crystal monochromator Si(111) to 60% of the rocking curve maximum, using the beam-stabilization feedback control.

The simulations of the W L<sub>3</sub>-edge EXAFS spectra were performed using recently developed method, based on the joined use of classical MD simulations combined with *ab initio* EXAFS spectra calculations [1]. The MD simulations were performed in the NVT ensemble at 300 K using GULP3.1 code [14, 15] for a supercell 3×3×3, containing 324 atoms. A set of 4000 static atomic configurations was obtained during a simulation run of 20 ps with a time step interval of 0.5 fs. These configurations were further used to calculate the W L<sub>3</sub>-edge configuration-averaged EXAFS signals using *ab initio* real-space multiple-scattering FEFF8.2 code [16]. The complex exchange-correlation Hedin-Lundqvist potential and default values of muffin-tin radii, as provided within the FEFF8.2 code [16], were employed.

For  $\text{CaWO}_4$  we have used Senyshyn’s force-field model [17] (Table 1), which is able to describe structural, elastic and phonon properties. It consists of the pairwise interatomic potentials and the three body interaction. Note that the three body potential is required to stabilize [WO<sub>4</sub>] tetrahedra in the MD simulations. The atomic charges were taken from the DFT calculations and are equal to +2.0 for Ca, +1.68 for W and -0.92 for O atoms. Force-field models for  $\text{SrWO}_4$  and  $\text{BaWO}_4$  were constructed based on  $\text{CaWO}_4$  model (Table 1). The atomic charges were left unchanged, only the short range Buckingham, Morse and three body potential parameters were optimized to reproduce tungstate structure [6] and the highest phonon frequency corresponding to the W–O vibrations [8].

### 3. Discussion

The configuration-averaged W L<sub>3</sub>-edge EXAFS spectra  $\chi(k)k^2$  for three tungstates, calculated within the single-scattering (SS) and multiple-scattering (MS) approximations, are compared with the experimental data in Fig. 1. In the analysis of outer coordination shells the influence of the MS effects on the overall EXAFS spectrum should be always considered. However, as one can clearly see, the MS effects play only minor role in the EXAFS spectra for three tungstates, changing their amplitude less than 10%. The phase of the EXAFS spectra is described rather well by our theoretical model in all  $k$ -space range, while their amplitude is slightly overestimated, especially, at the end of the spectra. Note that some high-frequency contributions are not present

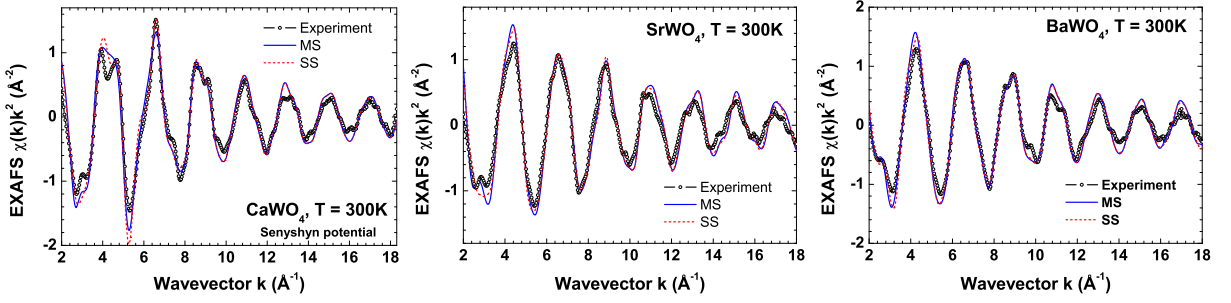


**Figure 1.** Comparison of the experimental and configuration-averaged W L<sub>3</sub>-edge EXAFS spectra  $\chi(k)k^2$  at 300 K for CaWO<sub>4</sub>, SrWO<sub>4</sub>, and BaWO<sub>4</sub>. Theoretical EXAFS spectra were calculated within the single-scattering (SS) and multiple-scattering (MS) approximations.

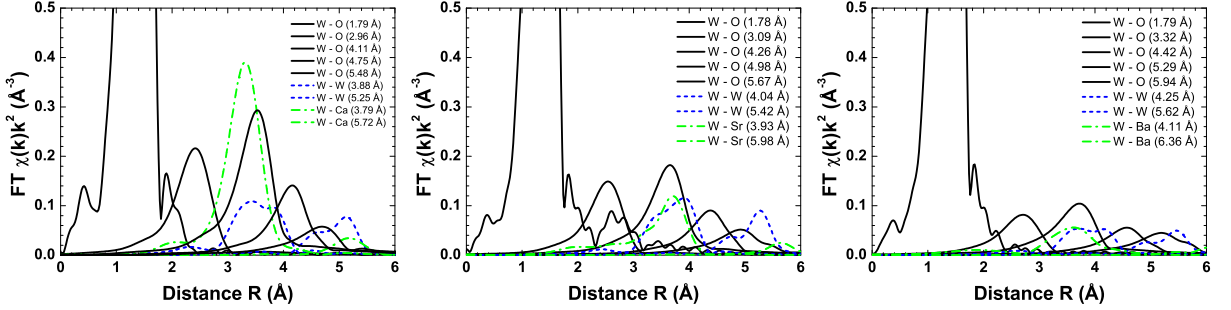


**Figure 2.** Fourier transforms (FT) of the W L<sub>3</sub>-edge EXAFS spectra  $\chi(k)k^2$  for separate coordination shells, calculated based on the structural parameters extracted from the results of the MD simulations.

in the configuration-averaged EXAFS spectra due to the limitation induced by the supercell size of 6 Å and resulting in the absence of contributions from more distant ( $>6$  Å) shells.

Because of rather good agreement between calculated and experimental EXAFS spectra, the accurate analysis of the second and further coordination shells can be reliably performed. The origin of peaks in Fourier transforms (FTs) of the EXAFS signals was identified for each shell (Fig. 2). To do that each peak in the radial distribution function (RDF), calculated till 6 Å from the MD simulations, was approximated by the Gaussian function, which depends on three parameters – position, amplitude and width. Such decomposition is possible, because peaks corresponding to the shells either do not overlap or overlap little. Using thus obtained set of structural parameters, the single-scattering EXAFS signals and their FTs for each coordination shell were calculated and are shown in Fig. 2.

As expected, the major contribution in FTs (the first peak at 1.3 Å in Fig. 2) comes from the four nearest oxygens at about 1.78-1.79 Å, forming the first coordination shell of tungsten. The mean square relative displacement values for the W–O bonds are small ( $4\text{--}6 \times 10^{-4}$  Å<sup>2</sup>) and are weakly influenced by the A<sup>2+</sup> ion type. This indicates strong W–O bonding in agreement with high vibrational frequencies observed by Raman spectroscopy [8, 9].

The outer shell contributions are noticeably smaller than from the first shell. The second peak is due to oxygen atoms located in the second coordination shell at about 2.96-3.32 Å. The next three overlapping peaks originate from A (A = Ca, Sr, Ba) atoms at 3.79-4.11 Å, O atoms at 4.11-4.42 Å, and W atoms at 3.88-4.25 Å. It is surprising that the most heavy tungsten atoms give the smallest contribution due to the thermal disorder. Note also a strong decrease of the amplitude for the peak, related to A-atoms, going from Ca to Ba. This effect can be explained

by the crystal lattice expansion due to an increase of the divalent cation size ( $R(\text{Ca}^{2+})=1.12 \text{ \AA}$ ,  $R(\text{Sr}^{2+})=1.26 \text{ \AA}$ ,  $R(\text{Ba}^{2+})=1.42 \text{ \AA}$ ). It leads to an increase of the separation between the two groups of the W–A distances: the differences are  $0.16 \text{ \AA}$  for  $\text{CaWO}_4$ ,  $0.20 \text{ \AA}$  for  $\text{SrWO}_4$ , and  $0.28 \text{ \AA}$  for  $\text{BaWO}_4$ . As a result, the strong amplitude damping of the corresponding total EXAFS signal occurs, and its FT peak decreases.

The next peak in FT at  $4.2\text{--}4.5 \text{ \AA}$  originates from the group of oxygen atoms located at  $4.75\text{--}5.29 \text{ \AA}$ . The three most distant peaks are due to the groups of tungsten atoms at  $5.25\text{--}5.62 \text{ \AA}$ , oxygen atoms at  $5.48\text{--}5.94 \text{ \AA}$ , and divalent atoms at  $5.72\text{--}6.36 \text{ \AA}$ .

## 4. Conclusions

In the present work we performed the W  $L_3$ -edge EXAFS study of the sheelite-type compounds ( $\text{CaWO}_4$ ,  $\text{SrWO}_4$ ,  $\text{BaWO}_4$ ) at room temperature. The experimental EXAFS spectra were interpreted using recently developed approach, based on classical molecular dynamics (MD) simulation combined with *ab initio* EXAFS spectra calculation [1].

The classical MD simulations in the NVT ensemble were performed at 300 K using the force-field potential models, which were developed for the  $\text{SrWO}_4$  and  $\text{BaWO}_4$  compounds based on the previously published model for  $\text{CaWO}_4$ . The good agreement between the experimental and calculated configuration-averaged EXAFS spectra allowed us to perform detailed analysis of the outer coordination shells contributions, leading to the following conclusions.

It was found that the MS contributions have minor influence (around 10%) on the W  $L_3$ -edge EXAFS signal in  $\text{AWO}_4$  compounds. The main part of the EXAFS signal comes from oxygen atoms in the first coordination shell. Besides, there are also noticeable contributions from the outer groups of oxygen atoms located up to  $6 \text{ \AA}$  and from A ( $\text{A} = \text{Ca}, \text{Sr}, \text{Ba}$ ) atoms. The latter decreases by going from Ca to Ba due to the crystal lattice expansion inducing the separation between the two A-atoms shells. The contribution from the heavy tungsten atoms is surprisingly small due to the thermal disorder.

## Acknowledgments

This work was supported by ESF Project 2009/0202/1DP/1.1.1.2.0/09/APIA/VIAA/141 and Latvian Government Research Grant No. 09.1518. The EXAFS measurements have been financed from the European Community's Seventh Framework Programme under grant agreement No. 226716 (Project I-20100098 EC).

## References

- [1] Kuzmin A and Evarestov R A 2009 *J. Phys.: Conf. Ser.* **190** 012024
- [2] Kalinko A, Evarestov R A, Kuzmin A and Purans J 2009 *J. Phys.: Conf. Ser.* **190** 012080
- [3] Anspoks A, Kuzmin A, Kalinko A and Timoshenko J 2010 *Solid State Commun.* **150** 2270
- [4] Kuzmin A, Efimov V, Efimova E, Sikolenko V, Pascarelli S and Troyanchuk I O 2011 *Solid State Ionics* **188** 21
- [5] Timoshenko J, Kuzmin A and Purans J 2011 *Centr. Eur. J. Phys.* **9** 502
- [6] Gurmen E, Daniels E and King J S 1971 *J. Chem. Phys.* **55** 1093
- [7] Hazen R M, Finger L W and Mariathasan J W E 1985 *J. Phys. Chem. Solids* **46** 253
- [8] Gallucci E, Goutaudier C, Bourgeois F, Boulon G and Cohen-Adad M T 2002 *J. Solid State Chem.* **163** 506
- [9] Černý P, Jelínková H, Zverev P G and Basiev T T 2004 *Prog. Quantum Electron.* **28** 113
- [10] Balerna A, Bernieri E, Burattini E, Lusi A, Kuzmin A, Purans J and Cikmach P 1991 *Nucl. Instrum. Meth. A* **308** 234
- [11] Kuzmin A and Purans J 2001 *Rad. Measurements* **33** 583
- [12] Kuzmin A, Kalendarev R, Purans J, Itie J P, Baudalet F, Congeduti A and Munsch P 2005 *Phys. Scripta* **2005** 556
- [13] Gracia L, Longo V M, Cavalcante L S, Beltran A, Avansi W, Li M S, Mastelaro V R, Varela J A, Longo E and Andres J 2011 *J. Appl. Phys.* **110** 043501
- [14] Gale J D 1996 *Philos. Mag. B* **73** 3
- [15] Gale J D and Rohl A L 2003 *Mol. Simulat.* **29** 291
- [16] Ankudinov A L, Ravel B, Rehr J J and Conradson S D 1998 *Phys. Rev. B* **58** 7565
- [17] Senyshyn A, Kraus H, Mikhailik V B and Yakovyna V 2004 *Phys. Rev. B* **70** 214306